

Intermediate Boson. III. Virtual-Boson Effects in Neutrino Trident Production

R. W. Brown*

Case Western Reserve University, Cleveland, Ohio 44106

and

R. H. Hobbs†‡

*Laboratory for Nuclear Science and Department of Physics,
Massachusetts Institute of Technology, Cambridge, Massachusetts 02139*

and

J. Smith§ and N. Stanko§

The Institute for Theoretical Physics, State University of New York at Stony Brook, Stony Brook, New York 11790

(Received 13 April 1972)

The production of lepton tridents by neutrinos in a Coulomb field is a sensitive test of the diagonal terms in weak-interaction theory. If a charged vector boson exists then it can participate in such reactions as a virtual particle or a real one if the incident beam energy is sufficiently high. A neutral vector boson with no magnetic moment cannot interact with the electromagnetic field; so it participates only as a virtual particle. We examine in this paper two different effects due to these bosons. First that they have different effective couplings which modify the $V-A$ interaction to a more general combination of vector and axial-vector currents. At this level changes in the over-all coupling strength are more important than retaining effects due to the virtual-boson propagators. The recent model of Weinberg belongs to this classification. Second, we investigate the propagator effect of a charged vector boson mediating the usual $V-A$ theory.

I. INTRODUCTION

With the advent of a high-energy neutrino beam at the National Accelerator Laboratory (NAL) exciting possibilities now exist for testing the theory of weak interactions. In particular the search for the charged intermediate vector boson will be continued at higher masses. We have already presented, in the first two papers in this series,^{1,2} the results of detailed calculations on the standard W -boson production reaction

$$\nu_\mu + Z \rightarrow \mu^- + W^+ + Z, \quad (1.1)$$

where Z may be a target proton, neutron, or nucleus. In particular, the energy and angular distributions of the μ^- and the μ^+ from the subsequent decay of the W^+ were given. Information about the μ^+ is readily determined once we know that the W^+ 's polarization is predominantly left-handed provided that it decays via the mode

$$W^+ \rightarrow \mu^+ + \nu_\mu. \quad (1.2)$$

In the event, however, that the W boson is too heavy to actually be produced as a real particle, the reaction

$$\nu_\mu + Z \rightarrow \mu^- + \nu_\mu + \mu^+ + Z \quad (1.3)$$

is still possible. This reaction, often called in the

literature neutrino trident production, has a very low threshold due to the smallness of the lepton masses. In standard $V-A$ theory with no intermediate vector boson the amplitude is represented by the two diagrams depicted in Fig. 1 where we use l to represent possible combinations of muons or electrons. If a charged vector boson exists then one should consider the three diagrams in Fig. 2. Other modifications of weak-interaction theory due to the possible existence of neutral vector bosons would give the diagrams in Fig. 3.

Several calculations have been published regarding the cross section for reaction (1.3) in standard $V-A$ theory. We mention in particular the paper of Czyż, Sheppey, and Walecka³ who obtained the asymptotic form of the cross section. This is determined by the coherent reaction where the target nucleus participates as a whole. Individual scatterings from the protons and neutrons in the nucleus are smaller by roughly a factor of $Z^{2/3}$. Assuming an exponential form factor for the target nucleus given by $F(q^2) = \exp(q^2/2\beta^2)$, where $q^2 < 0$, the asymptotic formula for reaction (1.3) is

$$\sigma \cong \frac{4Z^2\alpha^2G^2}{9\pi^3} E_1\beta \frac{\sqrt{\pi}}{2} \times \left[\frac{4}{3} \ln\left(\frac{2E_1\beta}{m_\mu^2}\right) - \left(\frac{16}{3} + \frac{2}{3}C + \frac{4}{3}\ln 2 + \frac{1}{15}\frac{\beta^2}{m_\mu^2}\right) \right]. \quad (1.4)$$

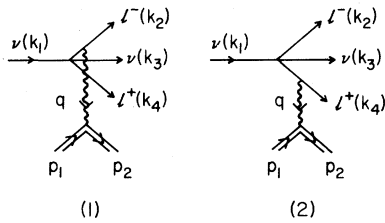


FIG. 1. Feynman diagrams for the reaction $\nu + Z \rightarrow l^- + \nu + l^+ + Z$ in a theory with a local four-fermion coupling.

In this expression E_1 is the neutrino beam energy, $\beta = \sqrt{5}/(1.2A^{1/3} \times 10^{-13} \text{ cm})$, and $C = 0.577$ is Euler's constant. This formula is valid above $E_1 = 10 \text{ GeV}$ and is very helpful in checking numerical calculations. The authors of Ref. 3 used numerical integration to obtain the cross section in the low-energy region where the asymptotic formula is not valid. Similar results have been given by Marinov *et al.*⁴ Recently detailed studies have been made by Fujikawa⁵ and by Løvseth and Radomski⁶ in order to obtain information on the energy and angular spectra of the two muons in the reaction. Such information is very important because other reactions, such as

$$\nu_\mu + n \rightarrow \mu^- + \pi^+ + \text{"anything,"} \quad (1.5)$$

have much larger cross sections than that of (1.3) and also yield two muons upon pion decay. Without detailed knowledge of the muon spectra it would seem impossible to design an experiment to distinguish (1.3) from (1.5). The paper of Løvseth and Radomski⁶ gives several tables of average energies, transverse momenta, etc., in the range of neutrino energies from 1.5 to 40 GeV. Production cross sections and averages are given for several nuclei as well as for individual production on protons and neutrons. The tables also give data on the off-diagonal reaction

$$\nu_\mu + Z \rightarrow \nu_e + e^+ + \mu^- + Z \quad (1.6)$$

and the diagonal reaction

$$\nu_e + Z \rightarrow \nu_e + e^+ + e^- + Z \quad (1.7)$$

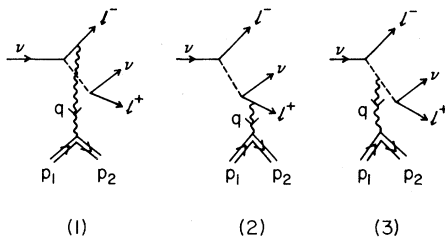


FIG. 2. Feynman diagrams for the reaction $\nu + Z \rightarrow l^- + \nu + l^+ + Z$ in a theory mediated by a charged vector boson.

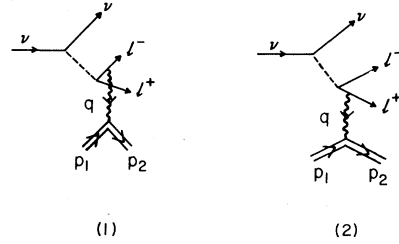


FIG. 3. Feynman diagrams for the reaction $\nu + Z \rightarrow l^- + \nu + l^+ + Z$ in a theory mediated by a neutral vector boson.

as well as on the diagonal reaction (1.3). Asymptotic cross sections for these processes have also been given in Ref. 3 assuming $V-A$ theory. For reaction (1.7) they found

$$\sigma \cong \frac{4Z^2\alpha^2G^2}{9\pi^3} E_1 \beta \frac{\sqrt{\pi}}{2} \times \left[\frac{4}{3} \ln \frac{2E_1}{\beta} - \left(\frac{22}{9} - \frac{2}{3}C - \frac{4}{3} \ln 2 \right) \right] \quad (1.8)$$

assuming the same exponential form factor given above. Both (1.4) and (1.8) show the general form of the cross sections as $\sigma \cong aE_1[\ln(E_1) - b]$ where a and b are constants. The corresponding neutrino lepton scattering cross sections ($\nu_e + e^- \rightarrow \nu_e + e^-$, for example) have the form $\sigma \sim s$, the total c.m. energy squared. In the production reactions $s = M_T^2 + 2M_T E_1$ where M_T is the mass of the target. However, in the coherent limit, the mass of the target is replaced by the inverse of the range of the nuclear potential which then sets the scale of the asymptotic formula. Naturally (1.8) is valid at lower energies than (1.4) and also gives a valuable check of numerical calculations. Energy and angular distributions of the leptons in the production processes have also been given by Koike, Konuma, Kurata, and Sugano⁷ and by Berkov, Voronina, and Shabalin.⁸ The main results from these investigations are that the μ^- in reaction (1.3) has higher average energy than the μ^+ and is produced at smaller angles. Also the distribution in the invariant mass of the $\mu^+ \mu^-$ pair is peaked for low masses. This is to be expected due to form-factor restrictions on top of the fact that the charged muon propagator denominators are small for low invariant masses and enhance the cross section in that region. We stress that the calculations mentioned above all assume the standard $V-A$ form of weak interaction theory and that the trident production processes essentially measure the diagonal as well as the off-diagonal weak interactions of leptons. Our only information on these processes at present comes entirely from the study of the beta decay of the muon which is an off-diagonal interaction. Although the

reaction $\bar{\nu}_e + e^- \rightarrow \bar{\nu}_e + e^-$ can possibly be measured directly the reaction $\nu_\mu + \mu^- \rightarrow \nu_\mu + \mu^-$ cannot be measured directly because we have no muon targets.

Recently there has been a great deal of interest in the diagonal terms in weak interaction theory from another point of view. Weinberg⁹ has proposed a model which involves both charged and neutral currents and shows some sign of being renormalizable. Studies by 't Hooft¹⁰ and Lee¹¹ of renormalization problems in theories with spontaneously broken Abelian gauge groups have been very promising. Although the general problem is not completely solved, Weinberg¹² has calculated some higher-order weak-interaction processes and shown them to be finite. His model makes specific predictions on the cross sections for diagonal weak lepton processes such as $\bar{\nu}_e + e^- \rightarrow \bar{\nu}_e + e^-$ and $\nu_e + e^- \rightarrow \nu_e + e^-$. Papers by 't Hooft¹³ and Chen and Lee¹⁴ have used the present experimental limits on these reactions to put bounds on the masses of the charged and neutral intermediate vector bosons in this model. Note that Weinberg's model reproduces the standard $V-A$ theory for off-diagonal reactions such as $\bar{\nu}_e + e^- \rightarrow \bar{\nu}_\mu + \mu^-$. The reason is that $\bar{\nu}_e + e^- \rightarrow \bar{\nu}_\mu + \mu^-$ cannot proceed via a neutral current. Some reactions such as $\bar{\nu}_e + e^- \rightarrow \bar{\nu}_e + e^-$ are changed because of the additional neutral current and some completely new interactions such as $\nu_\mu + e^- \rightarrow \nu_\mu + e^-$ are allowed for the first time. At present the experiments¹⁵ on the diagonal process-

es are not quite at the level where they have identified such reactions although refinements now in progress are expected to produce results for the total cross section for $\bar{\nu}_e + e^- \rightarrow \bar{\nu}_e + e^-$ in the near future. Even if Weinberg's model should turn out eventually to be nonrenormalizable it is imperative to pursue the experimental searches because standard $V-A$ theory is also nonrenormalizable and must require some modifications at high energies.

Neutrino trident production is yet another way of testing models such as those of Weinberg; in particular, allowing one to check on the presence of neutral currents. Since the neutrino beams at all of the large accelerators are mainly composed of ν_μ 's an ideal reaction to study is

$$\nu_\mu + Z \rightarrow \nu_\mu + e^+ + e^- + Z. \quad (1.9)$$

Normally the production of an electron pair is only allowed by an electron neutrino via the reaction (1.7). The small contamination in the beam by ν_e 's produced via the decay $K^+ \rightarrow \pi^0 + e^+ + \nu_e$ may be troublesome and prevent one from separating the two reactions on the basis of total cross section measurements alone. Therefore it is desirable to know the energy and angular distributions of both reactions (1.7) and (1.9). This is one of the motivations for the present paper.

If we now examine Weinberg's Lagrangian¹² and write out the relevant terms for trident production, we find¹⁶

$$\begin{aligned} \mathcal{L}_{\text{eff}} = & \frac{ig}{\sqrt{2}} \bar{\nu}\gamma^\mu \left(\frac{1+\gamma_5}{2} \right) e W_\mu^\dagger + \frac{ig}{\sqrt{2}} \bar{e}\gamma^\mu \left(\frac{1+\gamma_5}{2} \right) \nu W_\mu \\ & + \frac{i}{(g^2 + g'^2)^{1/2}} \bar{e}\gamma^\mu \left[\left(\frac{1-\gamma_5}{2} \right) g'^2 + \frac{1}{2} \left(\frac{1+\gamma_5}{2} \right) (g'^2 - g^2) \right] e Z_\mu + \frac{1}{2} i (g^2 + g'^2)^{1/2} \bar{\nu}\gamma^\mu \left(\frac{1+\gamma_5}{2} \right) \nu Z_\mu. \end{aligned} \quad (1.10)$$

Here g and g' are independent coupling constants related to the Fermi coupling constant G and the vector-meson masses M_W and M_Z by

$$\begin{aligned} \frac{G}{\sqrt{2}} &= \frac{g^2}{8M_W^2} \\ &= \frac{g^2 + g'^2}{8M_Z^2}. \end{aligned} \quad (1.11)$$

W_μ and Z_μ are the field operators for the charged and neutral bosons, respectively. It is now possible to make an exact calculation of the diagrams shown in Figs. 2 and 3 using this effective Lagrangian. However, the vector-boson masses in this model are already very large. Indeed, Weinberg¹² predicts that $M_W \geq 40$ GeV and $M_Z \geq 80$ GeV. Under such circumstances the effects due to the virtual-boson propagators are extremely small and the

square of (1.10) can be reduced to an effective local four-fermion interaction by taking the limit of M_W^2 and M_Z^2 large compared to all other invariants in the problem. The resulting Lagrangian is an admixture of vector and axial-vector currents. It is not however the usual $V-A$ theory. Such a reduction has been made by Chen and Lee,¹⁴ who introduced a parameter $\sin\theta = g'(g^2 + g'^2)^{-1/2}$. In the local limit the masses M_W^2 and M_Z^2 from the propagators combine with the coupling constants according to (1.11) leaving an effective four-fermion Lagrangian depending upon G and $\sin\theta$. Although it is still an admixture of charged and neutral currents a Fierz transformation can be performed to write all the possible terms in the charge retention form. The resulting effective Lagrangians for the diagonal processes now have the same form but have different values for their coupling strengths. For example the process $\bar{\nu}_e + e^- \rightarrow \bar{\nu}_e + e^-$ has the effective

Lagrangian

$$\mathcal{L}_{\text{eff}} = \frac{G}{\sqrt{2}} \bar{e} \gamma_{\mu} (C_V + \gamma_5 C_A) e \bar{\nu}_e \gamma^{\mu} (1 + \gamma_5) \nu_e, \quad (1.12)$$

with

$$C_V = \frac{1}{2} + 2 \sin^2 \theta, \quad (1.13)$$

$$C_A = \frac{1}{2}. \quad (1.14)$$

In standard $V-A$ theory one can also write the Lagrangian in the form (1.12) where $C_V = C_A = 1$. Similarly the process $\nu_{\mu} + e^{-} \rightarrow \nu_{\mu} + e^{-}$ has an effective Lagrangian

$$\mathcal{L}_{\text{eff}} = \frac{G}{\sqrt{2}} \bar{e} \gamma_{\mu} (C'_V + \gamma_5 C'_A) e \bar{\nu}_{\mu} \gamma^{\mu} (1 + \gamma_5) \nu_{\mu}, \quad (1.15)$$

with

$$C'_V = \frac{1}{2} - 2 \sin^2 \theta, \quad (1.16)$$

$$C'_A = \frac{1}{2}. \quad (1.17)$$

This process is forbidden in $V-A$ theory.

The fact that all these Lagrangians assume the general form (1.12) and (1.15) is easy to understand. We know that neutrinos are left-handed and antineutrinos are right-handed. This means that the $\bar{\nu}\nu$ combination must be $\bar{\nu}\gamma^{\mu}(1+\gamma_5)\nu$ so the lepton part can only have vector and axial-vector terms. It would therefore be very useful to have results for the neutrino trident production processes for an arbitrary combination of vector and axial-vector couplings, not just the $V-A$ combination known from the work of the previous authors. We give results in this general form so that they remain valid for any model of trident production processes. Of course the off-diagonal trident production process (1.6) still remains $V-A$ so we concentrate on the diagonal processes which give electron and muon pairs.

The analysis above is based upon the neglect of the boson propagator. This will be correct if the boson mass is very large. In the event that these models are misleading and vector bosons exist with masses in the range from 2 to 10 GeV then they will be copiously produced at NAL. There is, however, a region where the direct production process (1.1) is near threshold and has a cross section comparable to the neutrino trident production cross section (1.3) which is enhanced by the virtual-boson propagator. In this region the timelike boson propagator in diagram (1) of Fig. 2 will be small and enhance the cross section for the virtual-boson process. In order to understand these effects in more detail we also calculate the cross section for the diagrams of Fig. 2. Because the three diagrams involved lead to a tremendous number of terms when we square the matrix element

we have chosen a very simple model. We assume that a charged boson mediates the standard $V-A$ theory with the coupling constant relation $G/\sqrt{2} = g^2/M_W^2$. This avoids the complications due to the presence of neutral currents. A discussion of this calculation is also given in this paper. Note that virtual-boson effects arising from the presence of a neutral boson are very easy to calculate because if the neutral boson has no magnetic moment it does not interact with the electromagnetic field.

The outline of this paper is as follows. In the next section we calculate the cross sections and energy and angular distributions for the reactions

$$\nu_e + Z \rightarrow \nu_e + e^+ + e^- + Z$$

and

$$\nu_{\mu} + Z \rightarrow \nu_{\mu} + e^+ + e^- + Z.$$

The former is allowed by both the $V-A$ theory and Weinberg's model whereas the latter is only allowed by Weinberg's model. We give our results for arbitrary combinations of C_V and C_A so that other values can be used if required. Although Weinberg's model was originally formulated as a model involving electrons and not muons it is clearly of interest to know the general results for muons also. Therefore in Sec. III we carry out analogous calculations for the reaction $\nu_{\mu} + Z \rightarrow \nu_{\mu} + \mu^+ + \mu^- + Z$. We give the results for an arbitrary combination of C_V and C_A and compare the $V-A$ predictions with those of a hypothetical case where $C_V = 1.2$ and $C_A = 0.5$. This section is longer because incoherent scattering is not negligible near threshold so results are given for production of muon pairs off protons and neutrons as well as off the coherent nucleus. Section IV contains a discussion of effects due to the presence of a virtual charged intermediate boson. Finally in Sec. V we give our conclusions.

II. PRODUCTION OF ELECTRON PAIRS

In this section we study the reaction

$$\nu(k_1) + Z(p_1) \rightarrow e^-(k_2) + \nu(k_3) + e^+(k_4) + Z(p_2) \quad (2.1)$$

assuming that the local four-fermion interaction is given by the effective Lagrangian

$$\mathcal{L}_{\text{eff}} = \frac{G}{\sqrt{2}} \bar{e} \gamma_{\alpha} (C_V + \gamma_5 C_A) e \bar{\nu} \gamma^{\alpha} (1 + \gamma_5) \nu. \quad (2.2)$$

The matrix element is comprised of the two diagrams shown in Fig. 1. It is straightforward to write down the matrix element assuming that the target is a spin-zero nucleus. The lepton part of the matrix element is (apart from constant factors)

$$M_\mu = \bar{u}_{(e)}(k_2) \left[\gamma_\alpha (C_V + \gamma_5 C_A) \frac{1}{-\not{k}_4 - \not{q} - \mu} \gamma_\mu + \gamma_\mu \frac{1}{\not{k}_2 + \not{q} - \mu} \gamma_\alpha (C_V + \gamma_5 C_A) \right] v_{(e)}(k_4) \times \bar{u}_{(v)}(k_3) \gamma^\alpha (1 - \gamma_5) u_{(v)}(k_1) \quad (2.3)$$

and the hadron part is the usual expression for the electromagnetic interaction of a spin-zero particle. The square of the matrix element therefore decomposes into two parts, one being the spin sum on the leptons, which is reasonably complicated so Veltman's SCHOONSCHIP¹⁷ algebraic computer program was used to carry it out, the other being the second-rank tensor for the nucleus, i.e.,

$$P^{\mu\nu} = 4F(q^2) p_1^\mu p_1^\nu, \quad (2.4)$$

where $F(q^2)$ is the nuclear electromagnetic form factor. We have employed several fits to $F(q^2)$ to allow cross checks with the work of previous authors. The standard forms used are the dipole fit,

$$F(q^2) = (1 - q^2 R_0^2/20)^{-2} \quad (2.5)$$

and the exponential fit,

$$F(q^2) = \exp(q^2 R_0^2/10), \quad (2.6)$$

where $R_0 = 1.2 A^{1/3} \times 10^{-13}$ cm. The more complicated but more realistic Fermi form factor is a two-parameter fit to the nuclear charge density

$$\rho(r) = \rho_F(r) = [1 + \exp(r - R)/b]^{-1},$$

where $R = 1.07 A^{1/3} \times 10^{-13}$ cm and $b = 0.57 \times 10^{-13}$ cm. The evaluation of $F(q^2)$ for the Fermi form factor is then carried out numerically. We have derived a parametrization of this form factor which enabled us to check some results in Ref. 6 without explicitly adding another integration to our programs. The expressions given in (2.5) and (2.6) have the same expansion for small values of $|q^2|$. However, they both overestimate the actual value of the cross section. In our previous work, we found it convenient to use another exponential fit, namely, (2.6) with $R_0 = 1.3 A^{1/3} \times 10^{-13}$ cm. This form factor falls off faster for larger $|q^2|$ and the total cross section calculated using it is much closer to the result calculated assuming the Fermi distribution than the corresponding results from (2.5) and (2.6). The dipole fit tends to overestimate the cross section by as much as 50%. We show the various form factor fits in Fig. 4. The point marked (a) gives the value of the square of the four momentum transfer at the threshold for production of $\mu^+ \mu^-$ pairs. One sees that this value is already very low. At any reasonable energy the minimum momentum transfer is already so small that we are

only sensitive to low values of $|q^2|$. In fact there is little cross section above $|q^2| = 0.1$ (GeV/c)². When using the Fermi fit we took advantage of this fact and made a cutoff at $|q^2| = 0.25$ (GeV/c)². The total cross section is given by

$$\sigma = \frac{Z^2 \alpha^2 G^2}{(2\pi)^6 2M_T E_1} \int \frac{d^3 k_2}{2E_2} \int \frac{d^3 k_3}{2E_3} \int \frac{d^3 k_4}{2E_4} \int \frac{d^3 p_2}{2E_{p_2}} \frac{1}{q^4} \times \delta^{(4)}(p_1 + k_1 - p_2 - k_2 - k_3 - k_4) P^{\mu\nu} M_\mu M_\nu^* \quad (2.7)$$

Although the problem of calculating the cross section from (2.7) is easy in concept it is rather difficult in practice due to the extreme peaking of the square of the matrix element in phase space. There are seven integrations required to evaluate the total cross section. These integrations were first carried out numerically working in the laboratory frame with laboratory angles and energies as variables. As a check, we reproduced one result of Løvseth and Radomski,⁶ namely, the total cross section for (1.3) with 40-GeV neutrinos incident on an iron target. Once we were satisfied that their answer was indeed correct we switched to using their integration variables. These are basically scalar products of the various momenta which

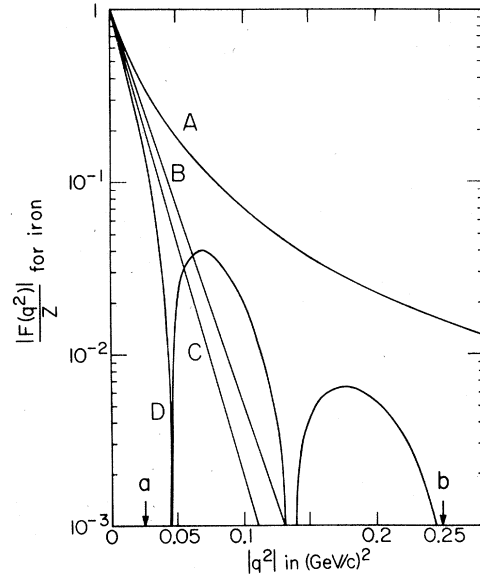


FIG. 4. Nuclear form factors commonly assumed for an iron nucleus. The curves correspond to the following: A is the dipole form factor used by Fujikawa (Ref. 5), B is the exponential form factor used by Czyż, Sheppey, and Walecka (Ref. 3), C is the exponential form factor used by Brown, Hobbs, and Smith (Ref. 2), and D is the Fermi form factor used by Løvseth and Radomski (Ref. 6). The arrows mark the threshold values for (a) the production of muon pairs and (b) the cutoff point for the Fermi form factor.

TABLE I. The total cross section in cm^2 for $\nu + Z \rightarrow \nu + e^+ + e^- + Z$ for coherent production off iron, divided into vector and axial-vector terms. We have multiplied by Z to facilitate comparison with the numbers given for $\nu + Z \rightarrow \nu + \mu^+ + \mu^- + Z$ in Table II. The final total cross section therefore requires another factor of Z .

Reaction	Energy in GeV	Coefficient of C_V^2 and C_A^2 in cm^2	Coefficient of $C_V C_A$ in cm^2	Cross section in cm^2 in $V-A$ theory where $C_V = C_A = 1$
$\sigma(\text{Fe})/26$	10	2.30×10^{-42}	2×10^{-44}	4.62×10^{-42}
	20	5.29×10^{-42}	9×10^{-44}	1.07×10^{-41}
	30	8.39×10^{-42}	3.9×10^{-43}	1.72×10^{-41}
	40	1.19×10^{-41}	4×10^{-43}	2.42×10^{-41}
	100	3.64×10^{-41}	-3.4×10^{-42}	6.94×10^{-41}
	140	4.89×10^{-41}	4.6×10^{-42}	1.02×10^{-40}

are then mapped into a new set of variables so that the integrand is smooth enough to allow the application of Monte Carlo integration in seven dimensions. For details we refer the reader to Appendix B of their paper. With the new variables substantially fewer points are required in the seven-dimensional phase space. Even then we required 3×10^5 points to generate smooth distributions.

We now study in detail the differences between the two reactions

$$\nu_\mu + Z \rightarrow \nu_\mu + e^+ + e^- + Z \quad (2.8)$$

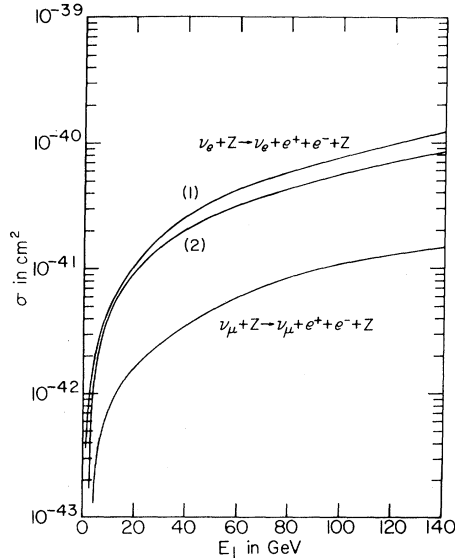


FIG. 5. Total cross sections for $\nu + Z \rightarrow \nu + e^+ + e^- + Z$ for incident neutrinos on iron. These cross sections are for the coherent case only and have been multiplied by Z^2 . (1) and (2) represent the reaction $\nu_e + Z \rightarrow \nu_e + e^+ + e^- + Z$ in $V-A$ theory and in Weinberg's model. The neutral current prediction for $\nu_\mu + Z \rightarrow \nu_\mu + e^+ + e^- + Z$ is also shown.

and

$$\nu_e + Z \rightarrow \nu_e + e^+ + e^- + Z. \quad (2.9)$$

Only a theory with neutral currents will allow reaction (2.8), whereas reaction (2.9) can proceed in both $V-A$ theory and in Weinberg's model. The analysis of Chen and Lee¹⁴ gave a value of $\sin^2\theta \lesssim 0.35$. We will take this upper limit for $\sin^2\theta$ and therefore use $C_V = -0.2$ and $C_A = 0.5$ for reaction (2.8). In the case of (2.9) we take $C_V = C_A = 1.0$, i.e., standard $V-A$ theory and also $C_V = 1.2$, $C_A = 0.5$ as determined by Weinberg's model.⁹

The results in this section are given only for coherent production off an iron nucleus. This is because the electron mass is so small that the process is essentially a coherent one. Effects due to incoherent production off individual protons and neutrons are therefore neglected. We present the total cross sections for reactions (2.8) and (2.9) in Fig. 5. For the values of C_V and C_A chosen above, the reaction initiated by the muon neutrino is generally one order of magnitude smaller in cross section than that initiated by the electron neutrino. If the electron contamination in the beam is smaller than one percent, then it may be possible to identify (2.8) on the basis of cross section measurements alone (assuming, of course, that $\sin^2\theta$ stays as large as 0.35). Table I gives the individual coefficients of C_V^2 , C_A^2 , and $C_V C_A$ in the formula for the total cross section. The values for C_V^2 and C_A^2 are identical while that for $C_V C_A$ is one hundred times smaller. Our over-all accuracy is around one percent which is the same order of magnitude as this coefficient. Hence it would be more realistic to drop this term entirely. The numbers we give are only representative of the order of magnitude of the coefficient and the fact that they fluctuate in sign should not be taken seriously. Why this is so will soon be obvious.

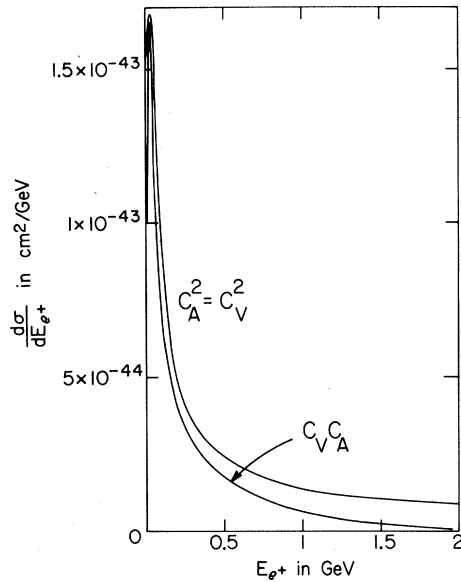


FIG. 6. $d\sigma/dE_{e^+}$ in cm^2/GeV versus E_{e^+} in GeV for production by 10-GeV neutrinos on iron with a coherent form factor. The total spectrum for arbitrary C_V^2 , C_A^2 and $C_V C_A$ can be found by adding the individual contributions. The electron spectrum is the same apart from $C_V C_A \rightarrow -C_V C_A$.

Figures 6 and 7 show the distribution in the positron energy for an arbitrary combination of C_V and C_A . For the electron distribution the only change is $C_V C_A \rightarrow -C_V C_A$. We see here that the magnitude of the C_V^2 and C_A^2 terms are identical which was to be expected because they differ only by terms proportional to the electron mass. The approximate matrix element for this process given by Chen and Lee¹⁴ also has identical contributions to C_V^2 and C_A^2 because they dropped all the mass terms. The change in the sign of the interference term means that its integrated contribution is very small. The relative numerical error is therefore rather large.

Fujikawa⁵ has given a helicity argument to explain the fact that the electron tends to have the

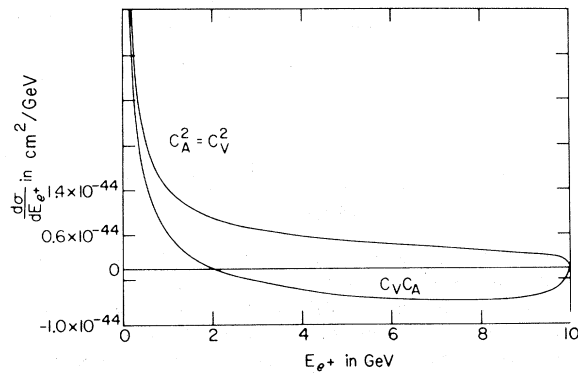


FIG. 7. Same as Fig. 6 for the rest of the energy scale.

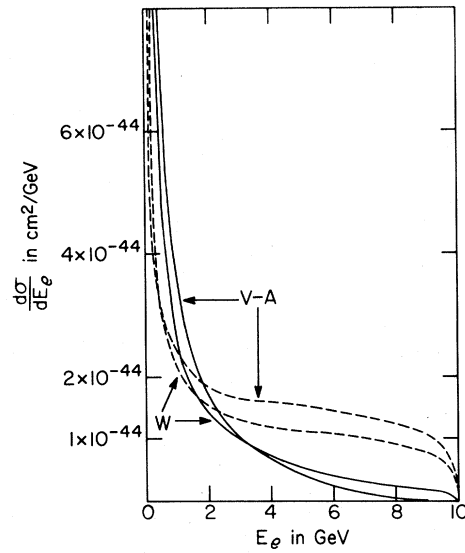


FIG. 8. $d\sigma/dE_e$ in cm^2/GeV versus E_e in GeV for $\nu_e + Z \rightarrow \nu_e + e^+ + e^- + Z$ and 10-GeV neutrinos on iron with a coherent form factor. The predictions of $V-A$ theory and the Weinberg model (W) are both shown. The solid lines give the positron distributions and the dashed lines the electron distributions.

larger average energy. This is also consistent with our numerical results. Since the electron tends to have the larger average energy, it is naturally produced in the more forward direction. Adding together the separate distributions produces results for the three cases, i.e., $\nu_e + Z \rightarrow \nu_e + e^+ + e^- + Z$ in both $V-A$ theory and Weinberg's model

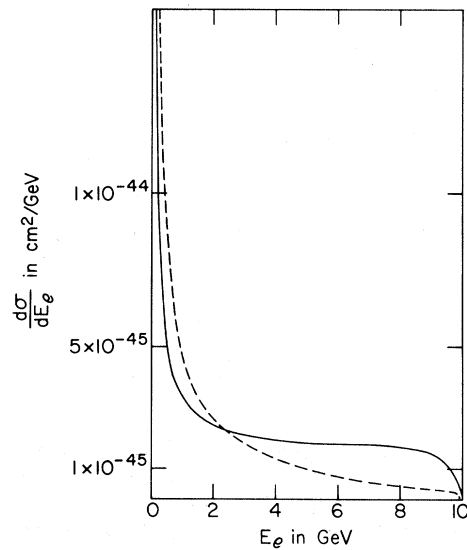


FIG. 9. Same as Fig. 8 for the reaction $\nu_\mu + Z \rightarrow \nu_\mu + e^+ + e^- + Z$ in Weinberg's model.

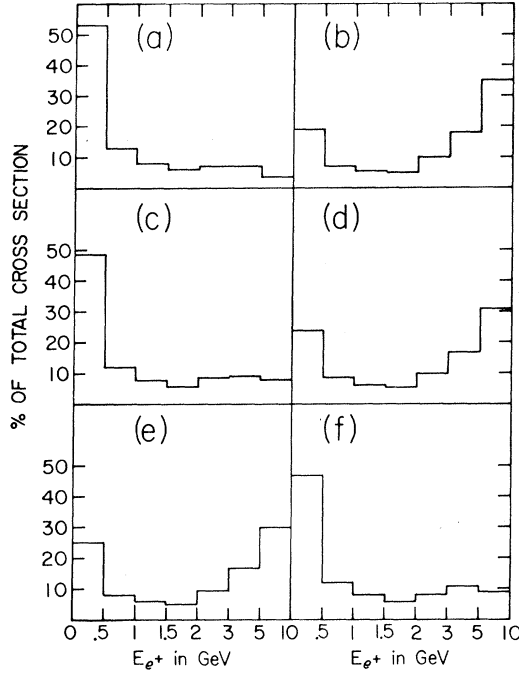


FIG. 10. Histograms of the percentage cross section per energy interval for the electron and the positron assuming 10-GeV incident neutrinos on an iron target. The curves (a) and (b) represent incident electron neutrinos in $V-A$ theory while (c) and (d) give the corresponding results for Weinberg's model. The neutral current results for muon neutrinos are shown in (e) and (f).

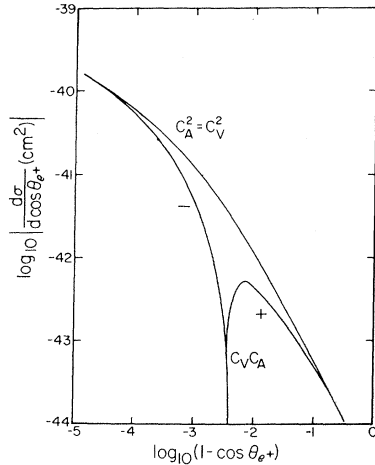


FIG. 11. $\log_{10}|d\sigma/d\cos\theta_{e+}|$ versus $\log_{10}(1-\cos\theta_{e+})$ for production by 10-GeV neutrinos on iron with a coherent form factor. The sign of the interference term is given so the total spectrum can be found by adding (or subtracting) the $C_V C_A$ term to the C_V^2 and C_A^2 terms. The results for the electron are the same except for $C_V C_A \rightarrow -C_V C_A$.

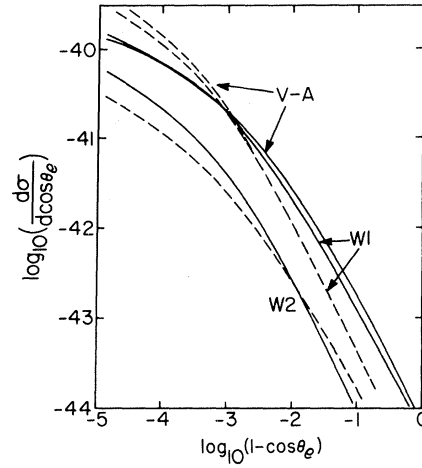


FIG. 12. $\log_{10}(d\sigma/d\cos\theta_e)$ versus $\log_{10}(1-\cos\theta_e)$ for the reactions $\nu_e + Z \rightarrow \nu_e + e^+ + e^- + Z$ in $V-A$ theory, in Weinberg's model (W1), and $\nu_\mu + Z \rightarrow \nu_\mu + e^+ + e^- + Z$ (W2). The target is iron with a coherent form factor and the beam energy is 10 GeV. The solid lines give the positron distributions and the dashed lines the electron distributions.

together with the neutral current prediction for $\nu_\mu + Z \rightarrow \nu_\mu + e^+ + e^- + Z$. These curves are shown in Fig. 8 and Fig. 9, respectively. Because it is very difficult to estimate the effect of cuts on the experimental energy distributions, we also give our results as histograms of the percentage cross section per energy interval. Figure 10 shows our results

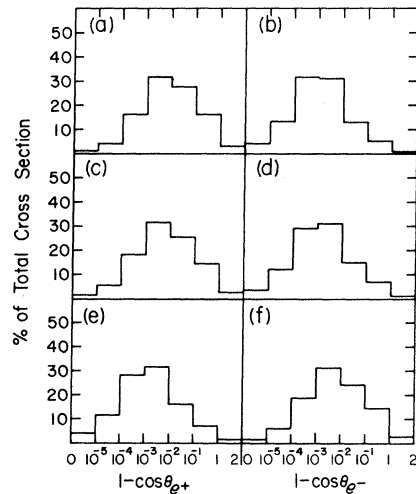


FIG. 13. Histograms of the percentage cross section per $\cos\theta$ interval for the electron and the positron assuming 10-GeV incident neutrinos on an iron target. The curves (a) and (b) represent incident electron neutrinos in $V-A$ theory while (c) and (d) give the corresponding results for Weinberg's model. The neutral current results for muon neutrinos are shown in (e) and (f).

for all three cases.

We would now like to comment on the change in over-all sign of the $C_V C_A$ term as we change from the e^- to the e^+ distribution. This is a reflection of charge-conjugation violation in the effective Lagrangian.⁵ The operation of charge conjugation applied to (2.2) switches the relative sign between C_V and C_A . As this is equivalent to switching the charges on the two leptons, we therefore anticipate a distribution in $C_V C_A$ for e^- which is just the opposite in sign from the distribution in $C_V C_A$ for e^+ . This means that the $C_V C_A$ term adds constructively at low energies for e^+ and destructively for e^- ; hence the larger average energy of the e^- . In the neutral current theory the sign of the $C_V C_A$ term is negative so now the e^+ obtains the larger average energy.

The angular distributions for the leptons are shown in Figs. 11 and 12, which demonstrate that the e^- angle is smaller than the e^+ in $V-A$ theory. The reason for this is again that the C_V^2 and C_A^2 contributions are identical while the $C_V C_A$ contribution changes sign in going from the e^- to the e^+ angular distribution. The corresponding results for the histograms of percentage cross section per $\cos\theta$ interval are shown in Fig. 13. It is obvious from all these results that there is only a small difference between the distributions and total cross sections for $\nu_e + Z \rightarrow \nu_e + e^+ + e^- + Z$ in standard $V-A$ theory and in Weinberg's model. The changes in the histograms are usually of the order of a few percent. However, there is a distinct difference between the energy and angular distributions for $\nu_\mu + Z \rightarrow \nu_\mu + e^+ + e^- + Z$ and $\nu_e + Z \rightarrow \nu_e + e^+ + e^- + Z$. The energy histograms show almost a complete reversal of the e^+ and e^- distributions for these reactions because the sign of the $C_V C_A$ term is now negative. This means that the neutral current tends to favor low-energy electrons at large angles and high-energy positrons at small angles. If the neutral current cross section from Weinberg's model is smaller than 10% of the charged current cross section, then the information we have given on the energy and angular distributions should still allow one to distinguish between the two cases.

III. PRODUCTION OF MUON PAIRS

In this section we study the reaction

$$\nu_\mu(k_1) + Z(p_1) \rightarrow \mu^-(k_2) + \nu_\mu(k_3) + \mu^+(k_4) + Z(p_2) \quad (3.1)$$

again assuming that it is described by a local four-fermion interaction with the effective Lagrangian

$$\mathcal{L}_{\text{eff}} = \frac{G}{\sqrt{2}} \bar{\mu} \gamma_\alpha (C_V + \gamma_5 C_A) \mu \bar{\nu} \gamma^\alpha (1 + \gamma_5) \nu. \quad (3.2)$$

Although Weinberg's model does not specifically

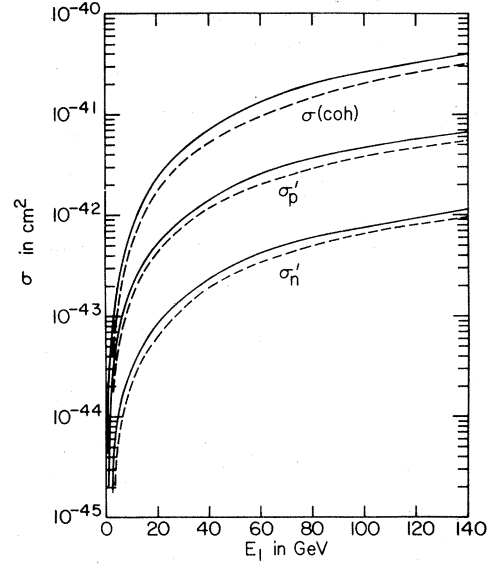


FIG. 14. Total cross sections for $\nu_\mu + Z \rightarrow \nu_\mu + \mu^+ + \mu^- + Z$ in two theories with $C_V = C_A = 1$ (solid lines) and $C_V = 1.2$, $C_A = 0.5$ (dashed lines). The curves represent the coherent cross section per proton on iron and the incoherent cross sections for scatterings by individual protons and neutrons. The final cross section is therefore $\sigma(\text{Fe}) = Z\sigma(\text{coh}) + Z\sigma'_p + N\sigma'_n$ where Z and N are the numbers of protons and neutrons in an iron nucleus.

include muons, it is clearly of interest to know the individual contributions of the vector and axial-vector currents. Generalizations of the model to include muons have been given by Gross and Jackiw¹⁸ and by Bouchiat, Iliopoulos, and Meyer.¹⁹ For muons, however, the incoherent production is not negligible compared to the coherent production for neutrino energies below 20 GeV. Hence we give results for both coherent and incoherent production. We consider the standard $V-A$ theory where $C_V = C_A = 1.0$ and a hypothetical Weinberg-type model where $C_V = 1.2$ and $C_A = 0.5$. The actual calculation is a trivial extension of the methods used in the previous section because we have kept all mass terms.

Due to the fact that the muon mass is much larger than that of the electron we are not justified in neglecting the incoherent production off individual protons. We take this into account very easily. The square of the matrix element decomposes into two parts. One is the spin sum of the lepton part which is identical to the result of the previous paragraph. However, the second part, the trace on the spin- $\frac{1}{2}$ hadron line, is now proportional to the second-rank tensor

$$P^{\mu\nu} = (G_E^2 + \tau G_M^2)/(1 + \tau) P^\mu P^\nu + G_M^2 (g^{\mu\nu} q^2 - q^\mu q^\nu). \quad (3.3)$$

TABLE II. Coherent (per proton) and incoherent total cross sections in cm^2 for $\nu + Z \rightarrow \mu^- + \nu + \mu^+ + Z$ divided into vector and axial-vector terms. To obtain the final total cross section for production on iron one takes the combination $\sigma(\text{Fe}) + Z\sigma'_p + N\sigma'_n$ where $Z=26$ is the number of protons and $N=30$ is the number of neutrons.

Reaction	Energy in GeV	Coefficient of C_V^2 in cm^2	Coefficient of C_A^2 in cm^2	Coefficient of $C_V C_A$ in cm^2	Cross section in cm^2 in $V-A$ theory where $C_V=C_A=1$
$\sigma(\text{Fe})/26$	4	4.09×10^{-44}	7.21×10^{-44}	-4×10^{-46}	1.12×10^{-43}
	10	2.89×10^{-43}	4.34×10^{-43}	-2×10^{-46}	7.23×10^{-43}
	20	1.01×10^{-42}	1.37×10^{-42}	2×10^{-45}	2.38×10^{-42}
	30	1.98×10^{-42}	2.55×10^{-42}	-2×10^{-45}	4.53×10^{-42}
	40	3.14×10^{-42}	3.91×10^{-42}	1×10^{-44}	7.06×10^{-42}
	50	4.37×10^{-42}	5.33×10^{-42}	2×10^{-44}	9.72×10^{-42}
	100	1.20×10^{-41}	1.38×10^{-41}	7×10^{-44}	2.58×10^{-41}
σ'_p	1.5	1.28×10^{-45}	1.88×10^{-45}	-9×10^{-48}	3.15×10^{-45}
	4	1.43×10^{-44}	1.79×10^{-44}	4×10^{-47}	3.23×10^{-44}
	15	1.53×10^{-43}	1.71×10^{-43}	9×10^{-46}	3.25×10^{-43}
	40	6.60×10^{-43}	7.01×10^{-43}	-5×10^{-45}	1.36×10^{-42}
	100	2.26×10^{-42}	2.34×10^{-42}	4×10^{-44}	4.64×10^{-42}
	140	3.43×10^{-42}	3.52×10^{-42}	-3×10^{-46}	6.95×10^{-42}
σ'_n	1.5	1.96×10^{-46}	2.67×10^{-46}	-3×10^{-48}	4.60×10^{-46}
	4	2.30×10^{-45}	2.74×10^{-45}	2×10^{-47}	5.07×10^{-45}
	15	2.48×10^{-44}	2.68×10^{-44}	2×10^{-46}	5.19×10^{-44}
	40	1.10×10^{-43}	1.14×10^{-43}	1×10^{-45}	2.25×10^{-43}
	100	3.68×10^{-43}	3.76×10^{-43}	-3×10^{-45}	7.40×10^{-43}
	140	5.55×10^{-43}	5.64×10^{-43}	1.2×10^{-44}	1.13×10^{-42}

Here we have defined $\tau = -q^2/4M_p^2$ and $P = p_1 + p_2$. The form factors for the nucleon are given by the standard dipole fit

$$\begin{aligned}
 G_E(\text{proton}) &= \frac{G_M(\text{proton})}{2.79} \\
 &= -\frac{G_M(\text{neutron})}{1.91} \\
 &= \left[1 - \frac{q^2}{0.71 (\text{GeV}/c)^2} \right]^{-2}, \quad (3.4)
 \end{aligned}$$

$$G_E(\text{neutron}) = 0. \quad (3.5)$$

We again calculated the total cross section by doing all seven integrations numerically. The cross section was also evaluated for coherent production using our exponential form factor given in Sec. II.

With these preliminaries out of the way we can now go directly to the results. In Fig. 14, we plot

the total cross section for (3.1) in standard $V-A$ theory with $C_V=C_A=1$ and with $C_V=1.2$ and $C_A=0.5$. These curves represent scattering from the coherent nucleus (where we have already multiplied by one factor of Z to aid in the comparison between the various results) and scattering by the individual protons and neutrons in the nucleus. We have included the effect of the Pauli principle in the form factors for the last two cases because it leads to a significant decrease in the total cross section for larger energies (and correspondingly smaller minimum momentum transfers). For details of this modification the reader is referred to Ref. 1. In case other values of C_V and C_A are needed we present the coefficients of the C_V^2 , C_A^2 , and $C_V C_A$ terms in Table II for a variety of energies and targets.

The total cross sections do not differ appreciably between the two models and the qualitative aspects

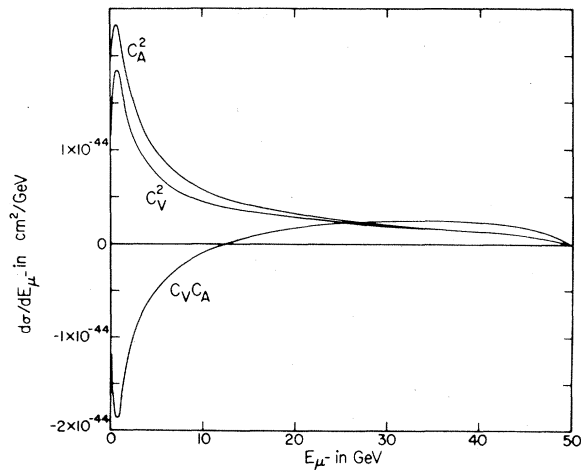


FIG. 15. $d\sigma/dE_{\mu^-}$ in cm^2/GeV versus E_{μ^-} in GeV for production by 50-GeV neutrinos on iron with a coherent form factor. The total spectrum for arbitrary C_V^2 , C_A^2 , and C_VC_A can be found by adding the individual contributions.

are similar to the difference between the corresponding electron results in Sec. II. In general the muon results are smaller than the electron results by approximately a factor of five due to the larger minimum momentum transfer in the muon case. Let us now examine the differential distributions in the energies and angles of the two muons. In Fig. 15 we plot $d\sigma/dE_{\mu^-}$ in cm^2/GeV versus E_{μ^-} in GeV for coherent production by 50-GeV neutrinos on iron with an exponential form factor. The total cross section for arbitrary C_V^2 , C_A^2 , and C_VC_A can be found by adding the individual contributions. In Fig. 16 we plot the corresponding curve for $d\sigma/dE_{\mu^+}$. One sees that the squares of the vector and axial-vector terms are almost the same. The small difference is due to muon mass effects as can be seen from the expression for the lepton

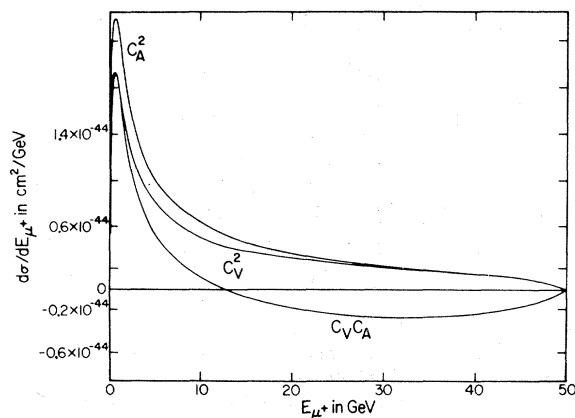


FIG. 16. Same as Fig. 15 for the positive muon.

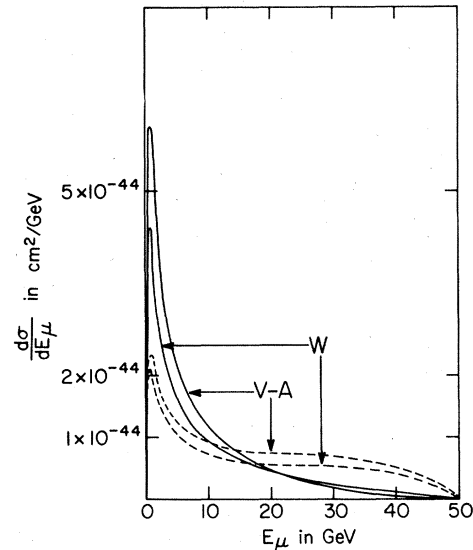


FIG. 17. $d\sigma/dE_{\mu}$ in cm^2/GeV versus E_{μ} in GeV for production by 50-GeV neutrinos on iron with a coherent form factor. The solid lines represent the μ^+ distributions and the dashed lines the μ^- distributions. The results for $C_V=1.2$ and $C_A=0.5$ are marked W .

trace where the coefficients of C_V^2 and C_A^2 differ only by terms proportional to the lepton mass.

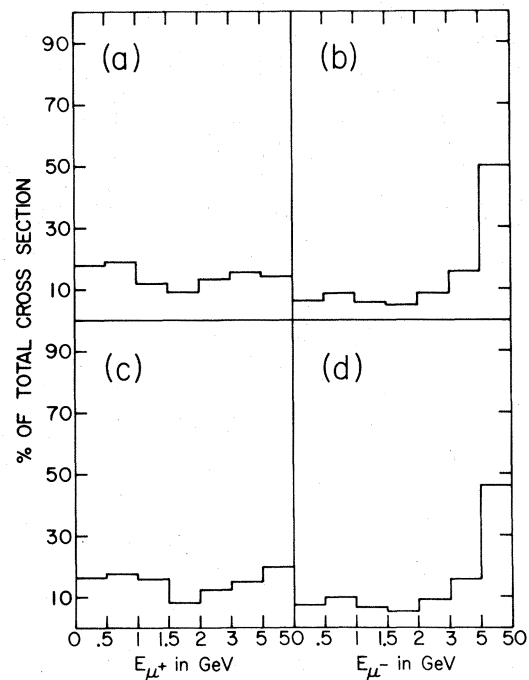


FIG. 18. Histograms of the percentage cross section per energy interval for positive and negative muons. These are drawn for 50-GeV incident muon neutrinos on an iron target. (a) and (b) are the results for standard $V-A$ theory while (c) and (d) are the results for $C_V=1.2$ and $C_A=0.5$.

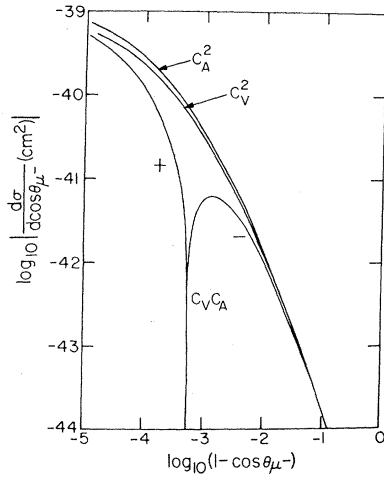


FIG. 19. $\log_{10}|d\sigma/d\cos\theta_{\mu^-}|$ versus $\log_{10}(1 - \cos\theta_{\mu^-})$ for production by 50-GeV neutrinos on iron with a coherent form factor. The sign of the interference term is given so that the total spectrum can be found by adding (or subtracting) the $C_V C_A$ term to the C_V^2 and C_A^2 terms. The results for the positive muon are the same except for $C_V C_A \rightarrow -C_V C_A$.

Again the $C_V C_A$ term completely reverses sign as we go from the μ^- to the μ^+ . This was to be expected because switching the charges of the muons corresponds to applying the operation of charge conjugation to the original Lagrangian. As we have already noted the Lagrangian is not invariant under this operation because the relative sign between C_V and C_A changes,⁵ which explains the change in the energy distributions. Upon addition, at least in standard $V-A$ theory, the curves for the μ^- interfere constructively at large energies and destruc-

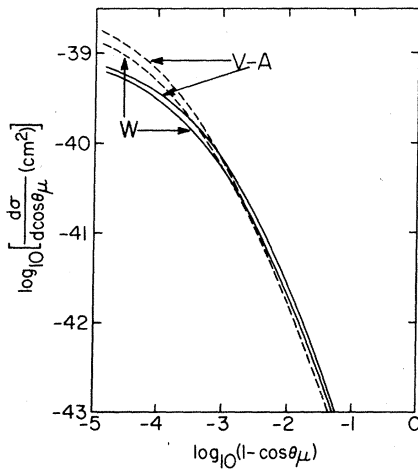


FIG. 20. $\log_{10}(d\sigma/d\cos\theta_{\mu})$ versus $\log_{10}(1 - \cos\theta_{\mu})$ for production by 50-GeV neutrinos on iron with a coherent form factor in $V-A$ theory and a theory with $C_V=1.2$ and $C_A=0.5$ (W). The solid lines are for the positive muon and the dashed lines for the negative muon.

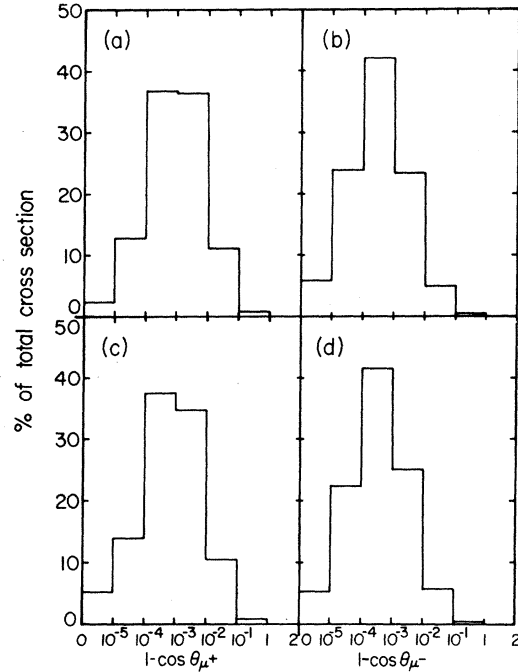


FIG. 21. Histograms of the percentage cross section per $\cos\theta$ interval for the reaction $\nu_{\mu} + Z \rightarrow \mu^{-} + \nu_{\mu} + \mu^{+} + Z$ on iron with a coherent form factor. (a), (b) represent the standard $V-A$ theory, and (c), (d) the hypothetical case when $C_V=1.2$ and $C_A=0.5$.

tively at small energies. For the μ^+ the reverse is true. Hence the μ^- receives a larger average energy than the μ^+ and it should therefore be pro-

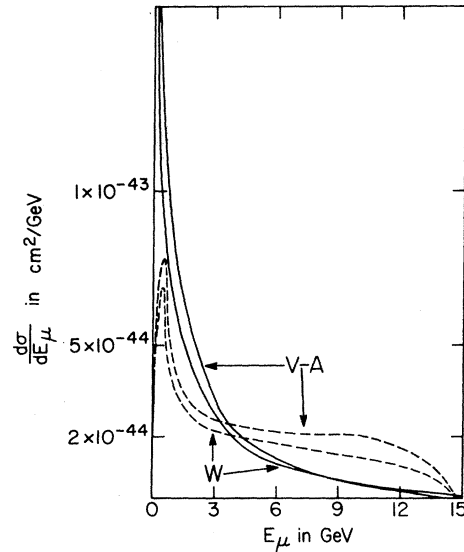


FIG. 22. $d\sigma/dE_{\mu}$ in cm^2/GeV versus E_{μ} in GeV for production by 15-GeV neutrinos off a proton in $V-A$ theory and a theory with $C_V=1.2$ and $C_A=0.5$ (W). The solid lines are for the positive muon and the dashed lines the negative muon.

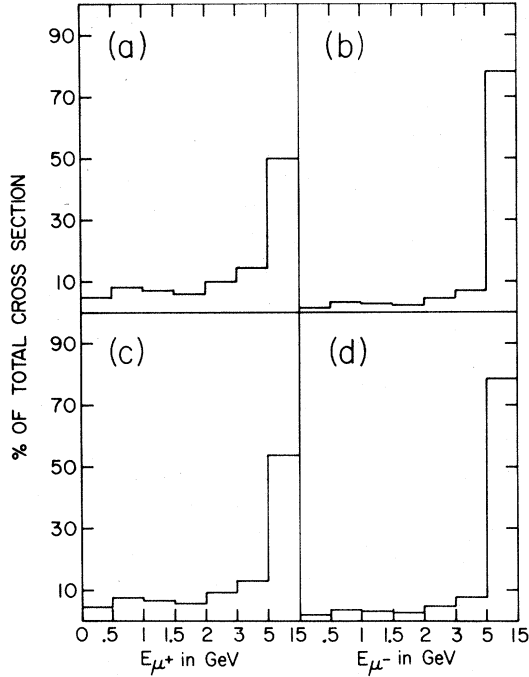


FIG. 23. Histograms of the percentage cross section per energy interval for the positive and negative muons. The neutrinos have 15-GeV energy and are incident on a target proton. (a), (b) are the V-A results and (c), (d) the results for $C_V=1.2$ and $C_A=0.5$.

duced at smaller angles. For illustration we have added the curves to compare the resulting energy distributions in the V-A theory where $C_V=C_A=1$ and in the model where $C_V=1.2$ and $C_A=0.5$. Figure 17 shows the spectra in the μ^- energy (dashed

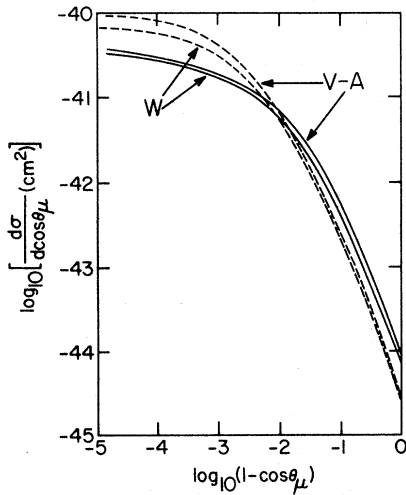


FIG. 24. $\log_{10}(d\sigma/d\cos\theta_\mu)$ versus $\log_{10}(1-\cos\theta_\mu)$ for production by 15-GeV neutrinos on a proton in V-A theory and a theory with $C_V=1.2$ and $C_A=0.5$ (W). The solid lines are for the positive muon and the dashed lines the negative muon.

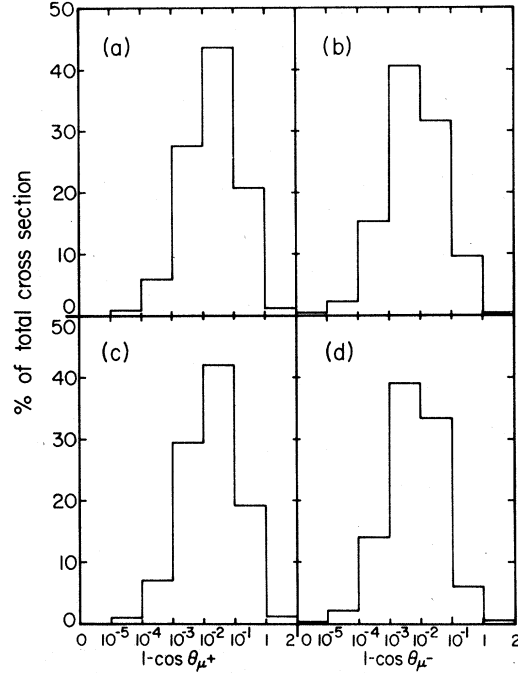


FIG. 25. Histograms of the percentage cross section per $\cos\theta$ interval for the reaction $\nu_\mu + p \rightarrow \nu_\mu + \mu^+ + \mu^- + p$ in the case of (a), (b) standard V-A theory and (c), (d) our model with $C_V=1.2$ and $C_A=0.5$.

lines) and the spectra in the μ^+ energy (solid lines). Our results are also given in histograms of the percentage total cross section per energy interval in Fig. 18.

If we now turn to the angular distributions they are generally peaked very strongly in the forward direction. Figure 19 shows $d\sigma/d\cos\theta$ for the coherent case. The corresponding results for the positive muon follow from $C_V C_A \rightarrow -C_V C_A$. The final distributions in V-A theory and in our hypothetical model can be found in Fig. 20. For convenience we also give our results as histograms of the percentage cross sections per $\cos\theta$ interval in Fig. 21. One notices that there is very little difference between the results from the two theories with this particular choice of C_V and C_A and, if there is an over-all normalization problem present in an experiment, it will be very difficult indeed to distinguish between them. However, if the sign of the $C_V C_A$ term were negative the distributions for the μ^- and μ^+ would switch over completely producing a dramatic change.

The corresponding results for scattering from individual protons and neutrons will now be given. In general, because the form factor does not decrease so fast in $|q^2|$, the distributions tend to favor larger angles. The individual contributions of the C_V and C_A terms follow the same pattern as in

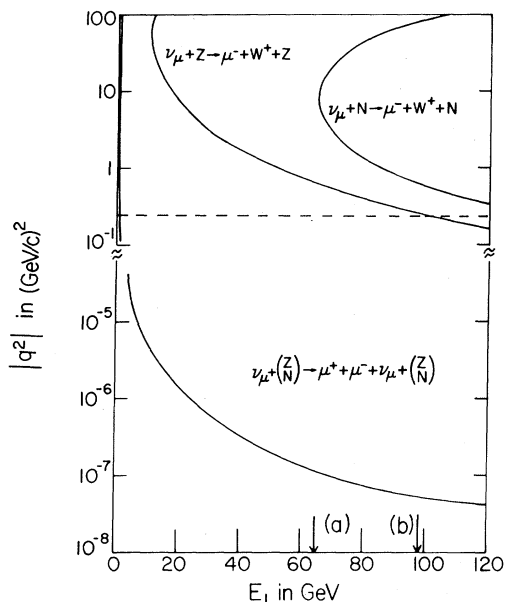


FIG. 26. Momentum transfer in $(\text{GeV}/c)^2$ versus the incident beam energy in GeV. The curves represent the kinematically allowed boundaries for the reactions indicated. The line at $|q^2| = 0.25 (\text{GeV}/c)^2$ represents the cut-off on the nuclear Fermi distribution. The arrows give the energy thresholds for (a) incoherent and (b) coherent W boson production with $M_W = 10 \text{ GeV}$.

the coherent case so we omit them here. The energy distributions in $V-A$ theory and a Weinberg-type model are given in Fig. 22. Figure 23 gives the relevant histograms. The analogous angular distributions are given in Fig. 24, and the histograms are given in Fig. 25. In general the neutron case is similar so we will not present the distributions for neutrons. As can be seen in Table II, the total cross sections for protons are larger than those for neutrons so the neutron makes only a 10% correction (except for very low beam energies). The proton calculations were made for 15-GeV incident neutrinos and we included a modification in the form factor to simulate the effect of the Pauli-principle suppression for small $|q^2|$.

IV. INTERMEDIATE BOSON EFFECTS

We would now like to examine the question of what happens when we include in our calculation the charged intermediate boson as the carrier of the weak interactions, i.e., the diagrams in Fig. 2. Before doing any calculations it is instructive to look at a plot of the momentum transfer to the nucleus versus the laboratory neutrino energy. Such a plot is given in Fig. 26. The boundaries drawn are for the reactions

$$\nu_\mu + Z \rightarrow \mu^- + \nu_\mu + \mu^+ + Z \quad (4.1)$$

and

$$\nu_\mu + Z \rightarrow \mu^- + W^+ + Z. \quad (4.2)$$

The integration over $|q^2|$ for fixed E_1 is taken from a $|q^2|_{\min}$ to a $|q^2|_{\max}$ although large values of $|q^2|$ are severely damped by the form factors. For (4.1) the difference between a target proton and a heavy target nucleus is almost unobservable so there is only one curve representing both cases. One sees that the minimum momentum transfer is extremely small. However, this is misleading in that gauge invariance forces a dramatic cancellation between the two graphs in Fig. 1 at these low values of $|q^2|$. A rough average value of $|q^2|$ found by weighting the cross section by $|q^2|$ is more like $10^{-3} (\text{GeV}/c)^2$ for the case of coherent production and approximately $10^{-1} (\text{GeV}/c)^2$ for incoherent production. The corresponding curves for reaction (4.2) are drawn for a boson mass of 10 GeV. Although the threshold for coherent production off a nucleus is much lower there is no cross section at these energies because the form factor is so small that we are completely justified in setting it equal to zero above $|q^2| = 0.25 (\text{GeV}/c)^2$. Hence the actual production threshold is in fact above the incoherent production threshold at 63 GeV. There the form factor effects are finite because the proton form factor falls off so slowly. However in the region from 63 GeV to 70 GeV the direct production cross section for reaction (4.2) is not very large. To give a precise number $\sigma'_p = 8.4 \times 10^{-43} \text{ cm}^2$ for $E_1 = 70 \text{ GeV}$ and $M_W = 10 \text{ GeV}$ and increases rather rapidly so that by $E_1 = 100 \text{ GeV}$, $\sigma'_p = 9 \times 10^{-40} \text{ cm}^2$. In contrast the cross sections for the trident produc-

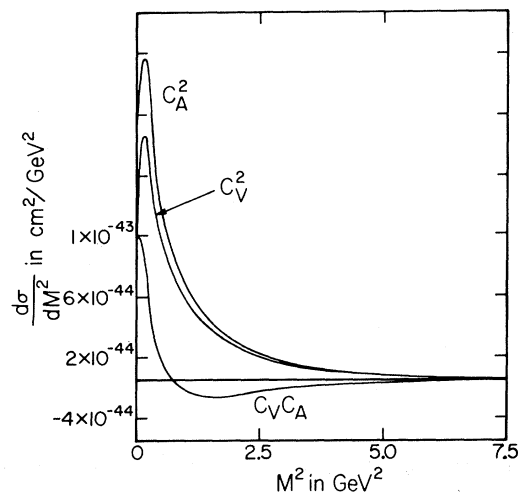


FIG. 27. The distribution in the invariant mass of the $\mu^+ \nu$ pair for production by 50-GeV neutrinos incident on an iron target and arbitrary C_V and C_A .

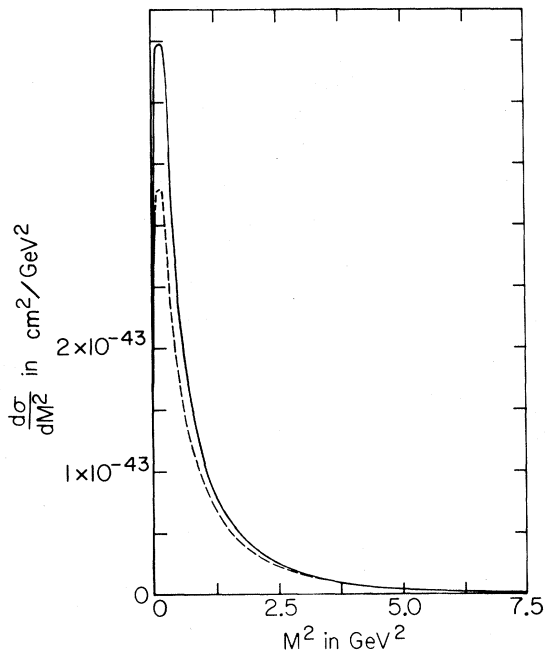


FIG. 28. The distribution in the invariant mass of the $\mu^+\nu$ pair. These curves are for neutrinos of 50-GeV incident on an iron target with a coherent form factor. The solid one is for $C_V = C_A = 1.0$ and the dashed one for $C_V = 1.2$ and $C_A = 0.5$.

tion reaction at 70 GeV are $\sigma'_b = 3 \times 10^{-42}$ cm² and $\sigma(\text{coh}) = 1.6 \times 10^{-41}$ cm². Obviously there is a region where the cross section for the direct production of $\mu^+\mu^-$ pairs is comparable to the cross section for the direct production of a W followed by its decay into $\mu^+\nu_\mu$. Our objective in this chapter is to investigate this region in some detail.

Normally the production of heavy mass objects in a Coulomb field is severely inhibited because the propagators are only enhanced for low masses.

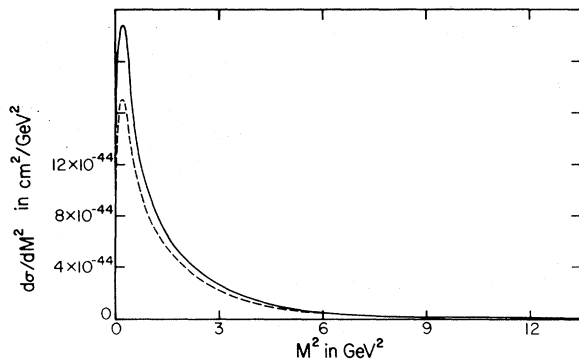


FIG. 29. The distribution in the invariant mass of the $\mu^+\nu$ pair for neutrinos of 15 GeV incident on a proton target. The solid curve is for $C_V = C_A = 1.0$ and the dashed curve for $C_V = 1.2$, $C_A = 0.5$.

For example, suppose we examine the calculation in Sec. III of the four-fermion reaction. The variable which corresponds to the mass of a hypothetical boson is $M^2 = (k_3 + k_4)^2$ which is timelike. If we bin this variable, then we can produce plots of $d\sigma/dM^2$ versus M^2 . Such plots are shown in Figs. 27–29 for coherent production on iron and production off a proton. The general feature of such plots is the low invariant mass of the dilepton system. One sees that the $C_V C_A$ term for the $(k_3 + k_4)^2$ distribution adds constructively at low masses and destructively at high masses. This is the same behavior as the energy distribution for the μ^+ . Although the beam energies are different in the two cases, it is obvious that the average value of M^2 is very low indeed in the coherent case and only slightly larger in the incoherent case. This is obviously controlled by the values allowed for $|q^2|$. There are regions in phase space where $|q^2|$ becomes very large so that the results are sensitive to large values in M^2 . However these regions contribute very little indeed to the final value of the cross section. As the general $|q^2|$ is extremely low, we can only enhance it by making cuts in the region of integration. Such cuts are very severe, however, because we lose most of our cross section. Also the average $|q^2|$ is so small that it will be very difficult to detect a recoil proton experimentally even if we restrict ourselves to larger $|q^2|$.

When the reaction is mediated by a vector boson, the distribution in $M^2 = (k_3 + k_4)^2$ will become infinite at the mass of the boson. Actually it does not really become infinite because the boson presumably has a definite lifetime and therefore a definite width. Dooher and Tausner²⁰ have examined a model where the intermediate charged boson was considered as a resonance with a certain width. They then calculated the cross section for the three diagrams in Fig. 2 in a modified Weizsäcker-Williams approximation. In this investigation they always chose beam energies above the production threshold and of course found total cross sections much larger than the usual trident production cross section. We would like to take a different viewpoint and stay slightly below the production of the boson as a real particle. We can only achieve this by actually calculating the cross section for the sum of the three graphs in Fig. 2 and introducing a cut in $(k_3 + k_4)^2$ so that we do not hit the point M_W^2 . We now give a brief account of this calculation.

The matrix element for the Feynman graphs depicted in Fig. 2 can be easily written down. We follow the same notation for the external four-vectors as in the previous section. However it is convenient to introduce the four-vectors character-

izing the boson propagators, i.e.,

$$k = k_3 + k_4 \quad (4.3)$$

and

$$k' = k_1 - k_2. \quad (4.4)$$

Note that $(k_3 + k_4)^2 > 0$ so it is a timelike vector and $(k_1 - k_2)^2 < 0$ so it is a spacelike vector. The amplitudes for the lepton parts of the three graphs are

$$M_\mu^I = \bar{u}_{(\nu)}(k_3)(-ig_W)\gamma_\alpha(1-\gamma_5)\nu_{(\mu)}(k_4)\bar{u}_{(\mu)}(k_2)(ie\gamma_\mu)\frac{i}{k_2^2 - M_W^2}(-ig_W)\gamma_\rho(1-\gamma_5)u_{(\nu)}(k_1)\frac{i}{k^2 - M_W^2}\left(-g^{\alpha\rho} + \frac{k^\alpha k^\rho}{M_W^2}\right), \quad (4.5)$$

$$M_\mu^{II} = \bar{u}_{(\nu)}(k_3)(-ig_W)\gamma_\alpha(1-\gamma_5)\frac{i}{-k_4^2 - M_W^2}(ie\gamma_\mu)\nu_{(\mu)}(k_4)\bar{u}_{(\mu)}(k_2)(-ig_W)\gamma_\rho(1-\gamma_5)u_{(\nu)}(k_1)\frac{i}{k'^2 - M_W^2}\left(-g^{\alpha\rho} + \frac{k'^\alpha k'^\rho}{M_W^2}\right), \quad (4.6)$$

and

$$M_\mu^{III} = \bar{u}_{(\nu)}(k_3)(-ig_W)\gamma_\beta(1-\gamma_5)\nu_{(\mu)}(k_4)\bar{u}_{(\mu)}(k_2)(-ig_W)\gamma_\rho(1-\gamma_5)u_{(\nu)}(k_1) \times \frac{i}{k^2 - M_W^2}\left(-g^{\beta\alpha} + \frac{k^\beta k^\alpha}{M_W^2}\right)(ie)\frac{1}{k'^2 - M_W^2}\left[g_{\alpha\lambda}(2k+q)_\mu - g_{\lambda\mu}(k+q)_\alpha - g_{\alpha\mu}k_\lambda\right]\left(-g^{\lambda\rho} + \frac{k'^\lambda k'^\rho}{M_W^2}\right). \quad (4.7)$$

We have written M_μ^{III} without including an anomalous magnetic moment. This is a necessary simplification because an arbitrary moment generates many extra terms when we square the diagrams. Our hope is that we can learn enough from this special case. We are partly justified in dropping the moment terms because diagram (3) is smaller in magnitude than diagrams (1) and (2). The sum of these three amplitudes is gauge-invariant, i.e.,

$$q^\mu(M_\mu^I + M_\mu^{II} + M_\mu^{III}) = 0. \quad (4.8)$$

Note that M_μ^{III} is not gauge-invariant by itself. Parts of M_μ^I and M_μ^{II} are needed to make the cancellation. In the limit that M_W becomes infinity all these terms drop out and we are left with the two diagrams in Fig. 1.

The squares of the above amplitudes contain a considerable number of terms. Again the calculation was done using Veltman's SCHOONSCHIP program.¹⁷ We folded these squares into the trace on the hadron line to give results for both the coherent and incoherent scattering cases. Unfortunately even with the simplification mentioned above, the resulting program is so long that we had to restrict ourselves to only a few actual runs on the computer. These runs were made at relatively low beam energies. First of all we checked that the results of this calculation were identical to the $M_W = \infty$ results in the local $V-A$ theory when the boson mass was sufficiently high. The relationship between the mass and threshold energy for its production is

$$E_1 \geq \frac{(M_W + M_p + \mu)^2 - M_p^2}{2M_p}, \quad (4.9)$$

so

$$M_W \leq (2M_p E_1 + M_p^2)^{1/2} - M_p - \mu. \quad (4.10)$$

Choosing a mass sufficiently large that Eq. (4.10) is violated yields the ordinary $V-A$ result. In order to see the effect of the W boson we must choose a mass so that Eq. (4.10) is satisfied and at the same time make cuts in $(k_3 + k_4)^2$ to avoid hitting the W -boson pole. Depending on the mass of the boson, we then find an increase in the total cross section and a change in the energy and angular distributions of the produced muons. In Table III we give the values of the total cross sections for 15-GeV neutrinos incident upon a proton target with different values for the intermediate boson mass. These results clearly show no change in cross section from the standard $V-A$ result when the boson

TABLE III. The total cross section in cm^2 for $\nu + p \rightarrow \mu^- + \nu + \mu^+ + p$ for 15 GeV incident neutrinos and various values of the mass of the charged intermediate vector boson in GeV. The distribution in $(k_3 + k_4)^2$ has been cut between $(M_W^2 - 0.2) \text{ GeV}^2$ and $(M_W^2 + 0.2) \text{ GeV}^2$ to avoid the pole. For comparison we also give the value in standard $V-A$ theory, where $M_W = \infty$.

M_W in GeV	$\sigma(M_W)$ in cm^2	$\sigma(M_W)/\sigma(M_W = \infty)$
2	2.0×10^{-42}	6.1
3	1.1×10^{-42}	3.3
4	3.6×10^{-43}	1.1
5	3.3×10^{-43}	1.0
∞	3.3×10^{-43}	1.0

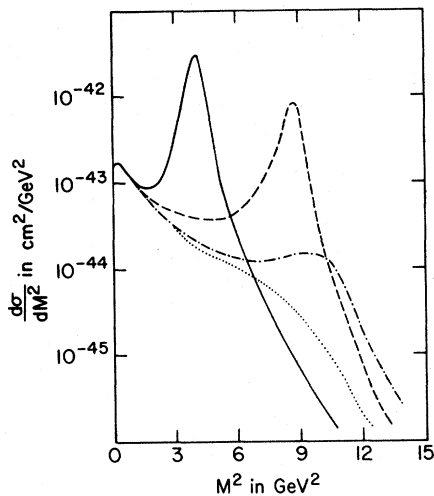


FIG. 30. The distribution in the invariant mass of the $\mu^+\nu$ pair for production off a proton with 15-GeV neutrinos. The solid, dashed, dot-dashed, and dotted lines are for W boson masses of 2, 3, 4, and 5 GeV, respectively. The values for the total cross section are given in Table III.

mass is large. For small boson masses, there is a change in cross section but this should only be considered a rough estimate in that we have not used any information on the width of the boson. To see the changes in the distributions, we take for illustration various boson masses ranging from 2 GeV through 5 GeV and plot the invariant mass distribution in Fig. 30. Choosing such low values for the mass produces significant changes in our distributions. Higher values would lead to smaller differences and it would not be so easy to see the changes in the graphs. We stress that the values chosen are for illustration only. Obviously if such

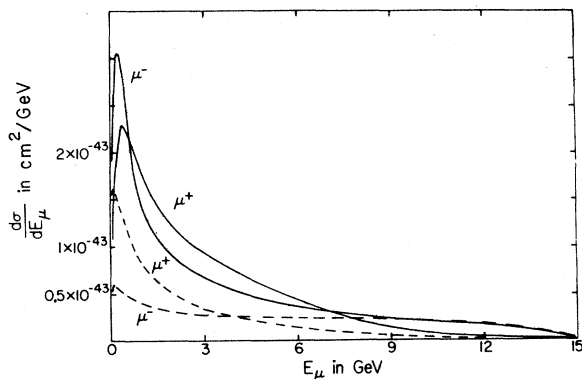


FIG. 31. Distributions in the muon energies for $\mu^+\mu^-$ production off a proton with 15-GeV neutrinos. The solid lines are the results for the calculation which includes a W boson with a mass of 2 GeV and a cutoff in $(k_3 + k_4)^2$ at 3.6 GeV. The dashed lines are the results from the standard trident production calculation in $V-A$ theory.

low-mass bosons exist they will be copiously produced at NAL. All the distributions shown have the characteristic low-mass peak and another peak of the square of the boson mass (if the boson can be produced as a real particle). When the boson mass is too large to be produced, there is some effect on the plots for large M^2 but only in the region where $d\sigma/dM^2$ is very small. The changes in the energy distributions for the muons are shown in Fig. 31. Now the μ^- has the low-energy peak, whereas the μ^+ is emitted with a higher average energy. This is the characteristic signal of the production of a W boson as a real particle. Our previous studies² showed that the W boson then tends to take all of the energy and be produced in a state of left-handed polarization. This means that the decay μ^+ is emitted with relatively large energy at a large angle. Our present example lies in the transition region between this case and the typical trident production distributions given previously. The angular distributions shown in Fig. 32 also show a more pronounced tendency for the μ^+ to be emitted at larger angles than before. However, the transition region is well behaved and the differences slowly disappear as we increase the boson mass. We have also checked that the same qualitative features occur in the coherent reaction although they are not quite so large due to the more rapid falloff in the coherent form factor.

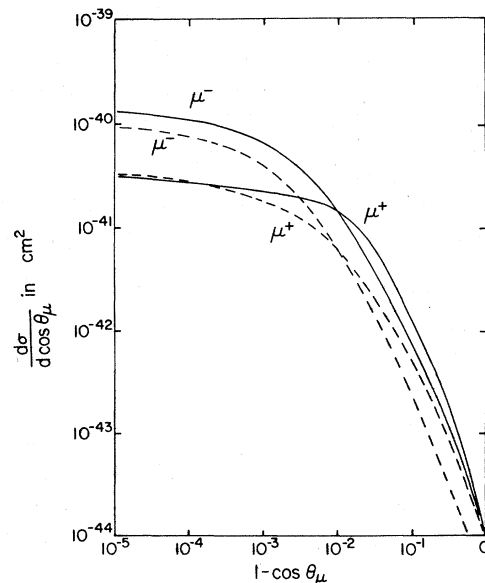


FIG. 32. The angular distributions of the muons for production off a proton with 15-GeV neutrinos. The solid lines are the results of the calculation which includes a W boson with a mass of 2 GeV and a cutoff in $(k_3 + k_4)^2$ at 3.6 GeV. The dashed lines are the results from the standard trident production calculation in $V-A$ theory.

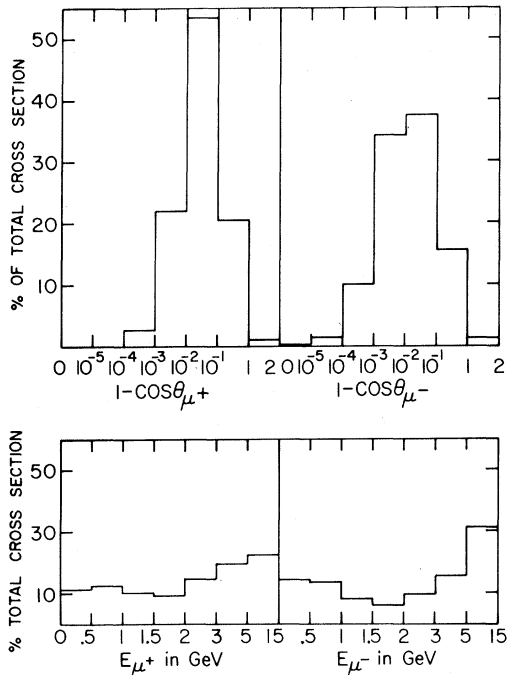


FIG. 33. Histograms of the percentage cross section per angle interval and per energy interval. The target is a proton with 15-GeV incident neutrinos. We have included a charged W boson with a mass of 2 GeV and a cutoff in $(k_3 + k_4)^2$ at 3.6 GeV.

Energy and angle histograms are given in Fig. 33.

The case of the neutral boson given in Fig. 3 is similar to the above. All one needs to do is multiply the individual diagrams by the two propagators. We have not done this because the model of Weinberg⁹ predicts a higher mass for the neutral boson than for the charged boson. Qualitatively we expect similar effects if we impose a cutoff on $(k_3 + k_4)^2$ so that we stay away from the pole. In case a neutral current does occur in nature, it would be more pleasing to actually detect it via the reaction $\nu_\mu + Z \rightarrow \nu_\mu + e^+ + e^- + Z$ before one takes into account the modifications to this reaction by the virtual propagators.

V. CONCLUSIONS

In this paper we concentrated on virtual-boson effects introduced through coupling constant changes and finite mass terms in neutrino trident production cross sections hoping that such effects will be observable at NAL energies. In the event that the standard $V-A$ theory does break down it is instructive to have some knowledge of possible types of nonlocal effects. First of all there is a distinct possibility that neutral currents begin to play some role which will allow certain reactions to proceed, i.e., $\nu_\mu + Z \rightarrow \nu_\mu + e^+ + e^- + Z$. Then

there is the possibility that these neutral currents modify the standard allowed reactions so that they are no longer of the $V-A$ type. In this event it is useful to know the lepton distributions for an arbitrary admixture of vector and axial-vector currents. This is only possible if the intermediate bosons are so massive that effects due to their propagators are negligible. If this is not the case then the neutrino trident cross sections have to be calculated from the basic Lagrangian coupling the lepton fields to the boson fields. In order to avoid the complexities due to neutral and charged bosons appearing at the same time we have examined these effects only in a theory where the $V-A$ interaction is mediated by a charged vector boson. The general case is much more complicated but it can be examined if and when the need arises. Needless to say the actual calculation of virtual neutral boson effects in reactions allowed by neutral currents would have been much easier to carry out. However due to their complexity such calculations should probably be postponed until some concrete evidence for neutral currents is found experimentally.

In general the total cross section for the reaction $\nu_\mu + Z \rightarrow \nu_\mu + e^+ + e^- + Z$ is not so large as that for $\nu_e + Z \rightarrow \nu_e + e^+ + e^- + Z$. One therefore needs to know the precise composition of the neutrino beam. If the contamination of ν_e 's is sufficiently small then any large production of e^+e^- pairs will be evidence for the presence of neutral currents. In the event that only a small number are produced, the data we have given on the energy and angular distributions should prove very useful. We warn the reader that radiative corrections to these distributions are not expected to be negligible.

The separate distributions we have given for the vector and axial-vector currents in the reactions should allow one to make a concise check of the $V-A$ nature of the weak interaction at these energies. We have concentrated only upon the trident processes where pairs of electrons and muons are produced. The reaction $\nu_\mu + Z \rightarrow \nu_e + e^+ + \mu^- + Z$ is therefore not covered by our analysis. We expect the same general features to occur, however, especially at reasonably large energies where the terms in the lepton mass are relatively small. Hence the μ^- should again have the larger average energy than the e^+ . This reaction is not modified by neutral currents and is expected to be of the $V-A$ type so the results in the paper of Løvseth and Radomski⁶ are applicable. In the event, however, that there is an over-all normalization problem it may be difficult to distinguish between specifically $V-A$ and a different admixture for the reaction $\nu_\mu + Z \rightarrow \nu_\mu + \mu^+ + \mu^- + Z$. The extreme case of $V+A$ will interchange the lepton distributions so that the

μ^+ receives the larger average energy. These distributions of course assume very heavy vector bosons and will be modified by the neutrino spectrum. When the actual spectrum is known it can easily be included.

In the event that a boson is actually produced as a real particle there is a sharp rise in total cross section and a completely new experimental signal. The μ^+ now receives the larger energy and the μ^- has the low-energy peak. Our study of the transition region shows that the changeover is relatively smooth. Hence the presence or absence of the boson is clearly to be decided upon by total cross section measurements. If the boson mass is large so that the cross section for actual production is on the same level as a typical trident production cross section then the problem of separation can only be solved by a detailed analysis of the two muon events. Anything which does not fit the $V-A$ trident production distribution is therefore evidence for the existence of a heavy boson. The less exciting possibility is that an experiment would find a few $\mu^+\mu^-$ events at the level of the $V-A$ theory and with the correct spectra. Such a discovery will only substantiate the standard $V-A$ theory and tell us nothing fundamentally new about the structure of weak interaction theory. However it would be the first time that the diagonal interactions involving the muon currents have actually been observed.

A last remark should be addressed to competing reactions with the same order-of-magnitude coupling strength. For example, we can get at least two muons from processes like $\nu_\mu + Z \rightarrow \mu^- + (Z+1) + \gamma \rightarrow \mu^- + \mu^+ + \mu^- + (Z+1)$ where the photon is emitted from the nucleus or the μ^- and produces a time-like pair of muons. However, for all the candidates we have considered, form-factor suppression and change-of-mass-scale in the cross sections as well as distinctly different muon signatures seem to indicate no real problems. Of course more detailed statements will be necessary when experimental results are finally obtained. Moreover, one must keep in mind the more serious problem of the pion decay background mentioned earlier.

ACKNOWLEDGMENTS

All of the authors would like to thank Brookhaven National Laboratory for hospitality at various periods during the course of this work. One of us (J.S.) would like to thank K. Fujikawa for an interesting discussion of the effects due to different vector and axial-vector currents in the neutrino trident production reactions. He would also like to thank J. Løvseth and M. Radomski for their very helpful correspondence and A. K. Mann for interesting comments.

*Work supported in part by the National Science Foundation GP-33119.

†Present address: United Aircraft Research Laboratory, Hartford, Connecticut 06108.

‡Work supported in part by the U. S. Atomic Energy Commission, Contract No. AT(30-1) 2098.

§Work supported in part by the U. S. Atomic Energy Commission, Contract No. AT(30-1) 3668B, and National Science Foundation, Grant No. GP-32998X.

¹R. W. Brown and J. Smith, Phys. Rev. D **3**, 207 (1971). We take this opportunity to correct typing errors in this paper. The three numbers for $\sigma(\text{Fe})/26$ with $\nu = -1, 0, +1$ at $E_1 = 200$ GeV in Table II were given as 6.64×10^{-3} , 6.90×10^{-3} , and 7.21×10^{-3} . These numbers were misread from the corresponding entries for $E_1 = 400$ GeV. They should read 5.90×10^{-3} , 6.07×10^{-3} , and 6.26×10^{-3} , respectively. We thank R. Linsker for pointing out this error. Also Fig. 5 is not in units for $(\text{GeV}/c)^2$ but rather in units where $M_W = 1$.

²R. W. Brown, R. H. Hobbs, and J. Smith, Phys. Rev. D **4**, 794 (1971).

³W. Czyż, G. C. Sheppey, and J. D. Walecka, Nuovo Cimento **34**, 404 (1964). References are given in this paper to earlier calculations made in the Weizsäcker-

Williams approximation. The statement that results calculated assuming dipole and exponential nuclear form factors bracket those calculated assuming a Fermi form factor is incorrect. The Fermi form factor falls off in momentum space faster than the particular exponential chosen by these authors so it leads to even smaller total cross sections.

⁴M. S. Marinov, Y. P. Nikitin, Yu. P. Orevkov, and E. P. Shabalin, Yad. Fiz. **3**, 678 (1966) [Sov. J. Nucl. Phys. **3**, 497 (1966)]. Neutrino trident production in a theory with a multiplicative lepton number has been considered by C. Y. Chang, Phys. Rev. Letters **24**, 79 (1970).

⁵K. Fujikawa, Ann. Phys. (N.Y.) **68**, 102 (1971), *ibid.* (to be published). See also Princeton thesis, 1970 for a discussion of the connection between $\nu_e e^-$ scattering and the reactions considered in this paper.

⁶J. Løvseth and M. Radomski, Phys. Rev. D **3**, 2686 (1971). There are two misprints in Appendix B of this paper. The left-hand side of Eq. (B10) should read $\sqrt{u_4}$ rather than u_4 and there is a $\cos\phi_4$ term missing in the equation for x_8 . There are also a few rather obvious misprints in the total cross section tables. We would like to thank both authors for their helpful comments on the best method to carry out the seven-dimensional in-

tegrations to compute the total cross section. Our preliminary runs using Gaussian quadrature gave answers which were too low by approximately 30%. Marinov *et al.* (Ref. 4) seem to have run into the same trouble because their answers are consistently 10% lower than those of Czyż *et al.* (Ref. 3). In these problems mappings should be made to reduce the peaking in the integration variables.

⁷K. Koike, M. Konuma, K. Karata, and K. Sugano, *Progr. Theoret. Phys. (Kyoto)* **46**, 1150 (1971); **46**, 1799 (1971).

⁸A. V. Berkov, L. M. Voronina, and E. P. Shabalin, *Yad. Fiz.* **14**, 416 (1971) [*Sov. J. Nucl. Phys.* **14**, 233 (1972)].

⁹S. Weinberg, *Phys. Rev. Letters* **19**, 1264 (1967).

¹⁰G. 't Hooft, *Nucl. Phys.* **B35**, 167 (1971).

¹¹B. W. Lee, *Phys. Rev. D* **5**, 823 (1972); see also B. W. Lee and J. Zinn-Justin, *ibid.* **5**, 3121 (1972); **5**, 3137 (1972); **5**, 3155 (1972).

¹²S. Weinberg, *Phys. Rev. Letters* **27**, 1688 (1971).

¹³G. 't Hooft, *Phys. Letters* **37B**, 195 (1971).

¹⁴H. H. Chen and B. W. Lee, *Phys. Rev. D* **5**, 1874

(1972). The term $-2(p \cdot p')(k \cdot k')$ in Eq. (11) of this reference should be deleted. Even with this correction the total cross section calculated from Eq. (11) is much too large. The approximation $m_e^2 \ll q^2$ is not very good because the important region in the q^2 integration is near $q^2 = (q^2)_{\min} = 4m_e^2/\omega^2$.

¹⁵R. Reines and H. S. Gurr, *Phys. Rev. Letters* **24**, 1448 (1970). H. S. Gurr, F. Reines, and H. W. Sobel, *Phys. Rev. Letters* **28**, 1406 (1972).

¹⁶Our basic notation and conventions are those of J. D. Bjorken and S. D. Drell, *Relativistic Quantum Mechanics* (McGraw-Hill, New York, 1964); and *Relativistic Quantum Fields* (McGraw-Hill, New York, 1965). In particular, $\hbar = c = 1$, $\alpha = e^2/4\pi$, and $\not{p} \equiv \gamma^\mu p_\mu$.

¹⁷M. Veltman, CERN report, 1967 (unpublished).

¹⁸D. J. Gross and R. Jackiw, *Phys. Rev. D* **6**, 477 (1972).

¹⁹D. Bouchiat, J. Iliopoulos, and Ph. Meyer, *Phys. Letters* **38B**, 519 (1972).

²⁰J. Doohar and M. Tausner, *Phys. Rev.* **142**, 1018 (1966).

Parametric Sum Rules for Electroproduction and Tests of Complex Scaling and Regge Behavior*

J. B. Healy

Rockefeller University, New York, New York 10021

(Received 31 May 1972)

Parametric dispersion relations which separately test complex scaling and Regge fits to the inelastic structure function $W_2(\nu, q^2)$ are found and evaluated. The numerical results indicate that precocious complex scaling is consistent with the present electroproduction data. The sum rule for the Regge fits is very restrictive and eliminates many of the fits proposed in the literature. The two fits which satisfy the sum rules are ones made by Pagels and by Preparata.

I. INTRODUCTION

Recently Khuri¹ has derived a new class of sum rules, or parametric dispersion relations, for off-shell Compton scattering. These sum rules follow from analyticity in two complex variables and complex scaling within the analyticity domain. Khuri and the present author² have evaluated several of these parametric dispersion relations; the results suggest that the sum rules are consistent with the concept of precocious complex scaling and that they provide tests of the Regge fits to the SLAC-MIT electroproduction data which go beyond the constraints imposed by the FESR (finite-energy sum rules). However, while some of these sum rules are more sensitive to the complex scaling hypothesis and others to the Regge fit used,

they do not allow totally independent tests of the two.

The purpose of this paper is to find and evaluate additional parametric dispersion relations which will furnish more stringent constraints on the behavior of the inelastic structure function νW_2 and which do not use both Regge behavior and complex scaling in the same sum rule. As in I, the sum rules we will consider also follow from analyticity in two complex variables. We will divide them into two classes. Those in class A will depend on the hypothesis of complex scaling, but not on the Regge fit used; those in class B will use only Regge input and analyticity and will provide new and rigorous restrictions on the Regge fits.

We have evaluated our sum rules using the SLAC-MIT electroproduction data^{3,4} on νW_2 and